Chapter 6
Planar Laser Induced Fluorescence Applied to Catalysis

Johan Zetterberg, Sara Blomberg, Jianfeng Zhou, Johan Gustafson and Edvin Lundgren

Abstract In this chapter we describe Planar Laser Induced Fluorescence (PLIF) to investigate the reactants or products in the vicinity of a catalyst at semi-realistic conditions. PLIF provides a 2D view of the gas-phase distribution of a pre-chosen gas. Here we present PLIF results from CO_2 and CO from the oxidation of CO into CO_2 by Pd single crystals and by various powder catalysts as well as from NH_3 from the oxidation of NH_3 above a Ag/Al_2O_3 powder catalyst. We describe our experimental set-up in detail, and the laser instrumentation needed to enable detectable gas fluorescence from CO_2, CO, and NH_3, respectively. Further, intensity corrections of the PLIF signal due to scattering and temperature effects are described. In the case of the CO oxidation, the results directly show the creation of a CO_2 boundary layer and thus a drastic change of the gas-phase composition close to the catalyst surface, illustrating the effect of gas diffusion and reaction speed, which in turn should affect the surface structure of the active catalyst. The 2D character of the PLIF images is used to investigate differences in catalyst activity by studying adjacent catalysts in the reaction cell during the reaction, and a solution to avoid spill-over effects between catalysts in the same reactor is presented. The results from PLIF images of CO of the same reaction show the corresponding depletion of the PLIF intensity above the catalyst, in accordance with observations from other techniques confirming the drastic difference between the gas composition close to the catalyst and at the inlet or outlet of the reactor. Finally we present NH_3 PLIF results from above a Ag/Al_2O_3 powder catalyst while the NH_3 is being oxidized in an oxidizing environment with the assistance of H_2.

J. Zetterberg · J. Zhou
Division of Combustion Physics, Lund University, 221 00 Lund, Sweden

S. Blomberg · J. Gustafson · E. Lundgren (✉)
Division of Synchrotron Radiation Research, Lund University, 221 00 Lund, Sweden
e-mail: edvin.lundgren@sljus.lu.se

© Springer International Publishing Switzerland 2017

J. Frenken and I. Groot (eds.), Operando *Research in Heterogeneous Catalysis*,
Springer Series in Chemical Physics 114, DOI 10.1007/978-3-319-44439-0_6

6.1 Introduction

Laser Induced Fluorescence (LIF) is a common, non-intrusive laser diagnostic technique for gas-phase studies in a number of research fields [1, 2] but is less known to the catalytic community. By the use of LIF, temperature, velocity and concentration of the probed gas can be determined [3]. The gas is probed with a laser tuned to a wavelength that matches an energy-level transition of the molecule of interest. If the wavelength is correctly chosen, no other molecular species will have an overlapping transition at that specific energy and the absorption cross section for the transition is high. When the molecule relaxes, fluorescent light is emitted which can be detected. This results in a strong LIF signal coming from one specific species, making concentration measurements on sub-ppm levels possible and LIF has therefore been used extensively in the investigation of the gas composition in flames and in other combustion-related environments.

In contrast, the use of LIF in catalysis-related research is comparably scarce. Previously, LIF has been used to study products or reactants such as OH [4–7], formaldehyde [8, 9], or naphthoquinone [10], in catalytic reactions. These molecules are easily accessible in the ultraviolet/visible region, making excitation and detection straightforward. However, a number of the more interesting molecules for catalysis such as CO, CO_2, and small hydrocarbons fluoresce in the mid-infrared region, making both excitations and detection more complicated. For instance, to detect CO_2 at elevated temperatures and realistic gas conditions, it is necessary to excite the molecule with a wavelength of 2.7 μm, demanding a high-energy laser with a respectable power and narrow line width (energy distribution). Furthermore, a fast, gateable infrared camera with the ability to detect the fluorescent light at 4.3 μm is necessary, since a fast subtraction scheme is needed to remove the otherwise completely dominating thermal background. Thus both laser source and detector camera are non-standard, making the experimental combination and the presented results in the present chapter rare or even unique. To obtain a 2D image of the gas-phase distribution above a catalyst, a laser sheet can be created, and the technique is then called Planar Laser Induced fluorescence (PLIF).

Motivated mainly by the difficulties in determining the active surface phase for Pd and Rh model catalysts during CO oxidation under semi-realistic conditions [11–24] and theoretical calculations [25–29], we have during recent years developed an experimental set-up suitable for probing the gas phase above the surface of an active catalyst using PLIF [30]. A simplified illustration of the PLIF experiment applied to catalysis is shown in Fig. 6.1 for the case of CO oxidation and detection tuned for CO_2, and the goal is to measure the amount of a reactant or product in the vicinity of the catalyst as we are changing the nature of the catalyst or the environments such as the gas pressure or sample temperature.

In the present chapter we describe our experimental set-up including the reactor and the gas flow system. We also explain which laser sources are used for a particular excitation of a molecule to induce a favorable fluorescence from the molecule of interest to enable PLIF observation of a catalytic reaction in which the molecule participates. Furthermore, the necessity of subtracting a thermal background for each

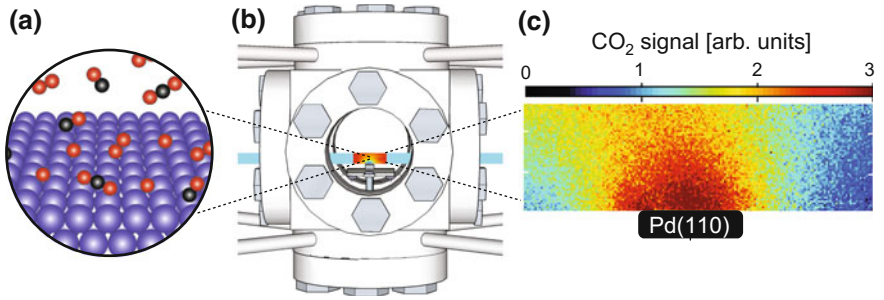

Fig. 6.1 A schematic of the PLIF measurements of the gas phase above a catalyst as presented in this chapter. **a** The adsorption and dissociation of O_2 and the adsorption of CO and production of CO_2. **b** The laser sheet (*blue*) that excites a vibrational-rotational level in the CO_2 molecules above the catalyst. **c** The resulting PLIF image of the CO_2 distribution above an active catalyst at elevated temperature and semi-realistic pressure

single PLIF measurement is described. In the first part we will focus on detecting the CO_2 production during CO oxidation above a single catalyst as well as above two or more catalysts probed simultaneously to demonstrate the 2D capabilities of the approach, and to possibly enable catalyst screening. These measurements also show, in a very direct way, the change of the gas-phase composition close to the catalyst surface as the catalyst becomes active. In the second part we describe how it is possible to probe the concentration of CO close to the catalyst surface during the CO oxidation and the complementary picture such measurements provide with respect to the CO_2 measurements. Finally, we will describe PLIF measurements tuned to fluorescence of NH_3 during its oxidation assisted by H_2 above a Ag/Al_2O_3 powder catalyst.

6.2 Experimental

6.2.1 Laser Set-Up and Laser Sheet

For each gas species probed in the present investigations, a unique combination of lasers and detectors was used. However, the general experimental set-up was the same in all cases, and a schematic overview is shown in Fig. 6.2a [30].

The infrared laser beam was in all cases formed into a laser sheet (6–15 mm high) by a cylindrical and a spherical lens, f = –40 mm and f = 150 mm, respectively (Fig. 6.2b), and was sent through the reactor just above the catalyst.

6.2.2 Reactor, Gas System, and Samples

In Fig. 6.2c an overall schematic of the set-up including the lasers, the mixing unit, the reactor, the IR-camera as well as the sample environmental control, for the case

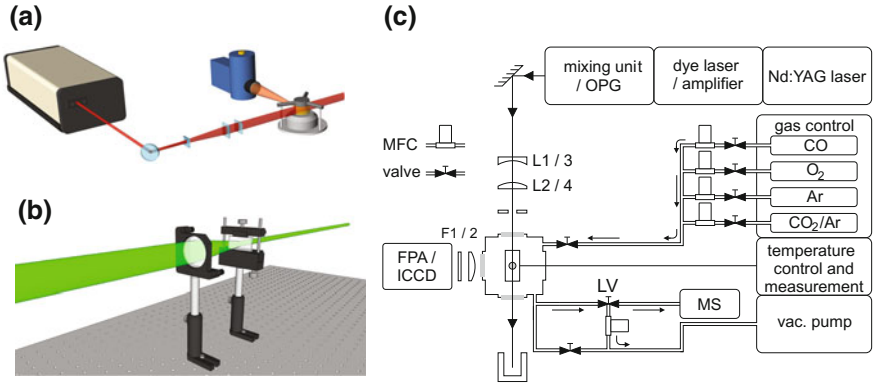

Fig. 6.2 **a** A schematic overview of the experimental set-up. **b** Illustration of transforming the point-like laser beam into a 2D sheet. **c** A more detailed description of the experimental set-up including the gas system and pumping units in the case of CO oxidation and CO_2 measurements

of CO_2 measurements, is shown. The reactor is a standard stainless-steel cube, fitted with CaF_2 windows allowing the laser to penetrate into the reactor and the fluorescence signal to reach to the detector. The samples are heated by a boron nitride heater and the surface temperature of the samples is measured by a standard type-C thermocouple and by an IR camera (FLIRP620). In the case of a single crystal, the samples were sputtered in a separate chamber before being introduced into the reactor and thus exposed to air and contaminations, while no pretreatment was performed for the powder-based samples. In all cases, the model catalysts were ramped up and down in temperature in an O_2, CO, and Ar-containing atmosphere to reduce the amount of contaminants. The feed gases were Ar, CO, O_2 and premixed 10% CO_2 in Ar for the CO_2 and CO measurements, and NH_3 and H_2 for the NH_3 measurements. The gases were introduced into the reactor cell via individual Bronkhorst mass-flow controllers (Bronkhorst EL-FLOW, 50 mln/min) that can vary the gas flow from 1 to 50 ml/min. To keep the pressure constant, a pressure controller (Bronkhorst EL-PRESS) was attached to the gas outlet. The gas composition was studied by a quadruple mass spectrometer (Pfeiffer PrismaPlus QMG220), connected to the reactor outlet via a leak valve.

6.2.3 LIF-General Considerations

The detected PLIF signal is dependent on a number of physical parameters which, in the linear excitation regime, can be described by

$$S_{LIF} = \eta_c E g f(T) \sigma_0 \chi_{\text{abs}} \frac{P}{k_B T} \phi. \tag{6.1}$$

η_c is the experimental collection efficiency, E is the laser energy, g is a function that describes the spectral overlap between the laser and the absorption spectral lineshape, $f(T)$ is the Boltzmann fraction, σ_0 is the absorption cross section of the probed gas, χ_{abs} is the mole fraction of the gas that together with $P/k_{\text{B}}T$ gives the gas number density, and ϕ is the fluorescence quantum yield. A more detailed description of the quantum yield related to IRLIF is given by Kirby and Hanson [31, 32]. The expression shows that the detected LIF signal is linearly dependent on the gas density and the fraction of molecules in the state from which the laser excites the molecule, $f(T)$.

As seen from the expression above, the signal is proportional to the number density of the probed gas. The number density N can be described by the mole fraction and the ideal gas law according to

$$N = \chi_{abs} \frac{P}{k_B T}. \tag{6.2}$$

This shows that the signal will decrease as a function of temperature. In order to analyze the influence of the temperature in the present measurements we measured the LIF signal at a constant pressure of 136 mbar of CO_2 while the temperature of the sample was increased from 120 to 290 °C. Figure 6.3 shows the calculated density of molecules/m^2 (dashed line) from the ideal gas law where the gas is assumed to have the same temperature as the sample together with the achieved LIF signal (solid line) 1.5 mm above the sample surface. The figure shows that the major signal decrease can be explained by the decrease of the gas number density, due to the increase of the temperature. However, the dependence on the population is not negligible and the LIF signal should be corrected for both, to represent the actual concentration distribution in the measurement.

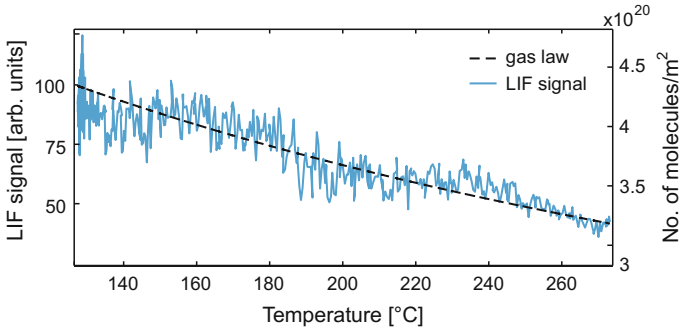

Fig. 6.3 The detected CO_2 LIF signal 1.5 mm above the sample (*full line*) as a function of temperature. The *dashed line* shows the calculated density of molecules as a function of temperature, the P(12) line was used for laser excitation

6.3 CO_2 Imaging

In Fig. 6.4a an excitation scan of CO_2 at 27 °C is shown. The present measurements were performed by exciting P12 in the $(00^00) \longrightarrow (10^001)$ transition of CO_2 as indicated in Fig. 6.4a. The energy diagram for the CO_2 molecule and the resulting fluorescence at 4.3 μm from the P12 level is shown in Fig. 6.4b.

In order to reach the P12 in the $(00^00) \longrightarrow (10^001)$ transition of the CO_2 molecule at 2.7 μm, the second harmonic at 532 nm from a Spectra Physics, PRO 290-10 Nd:YAG laser with a repetition rate of 10 Hz and an 8 ns pulse length was used to pump a Sirah PRSC-D-18 tunable dye laser using LDS 765 as dye. The residual of the fundamental beam (at 1064 nm) after the frequency doubling was difference-frequency mixed with the output of the dye laser (at 763 nm) in a $LiNbO_3$ crystal, yielding a tunable infrared laser beam at 2.7 μm, with a pulse energy of 5–8 mJ and a 5 ns pulse length. The bandwidth of the infrared laser beam was estimated in an earlier work to be 0.025 cm^{-1} [33].

Because of the fluorescence being in the infra-red region, the thermal background will interfere with the LIF signal. In Fig. 6.5 the schematics to remove the thermal background is shown as applied in the CO_2 measurements. The camera was triggered at 20 Hz, via a digital delay generator (Stanford Research Systems DG535), at every second exposure synchronized with the laser operated at 10 Hz, to subtract the background. The long radiative lifetime (100 μs) of the IR-transitions [34–36] was utilized to discriminate laser background and time jitter, by using a 15 μs time

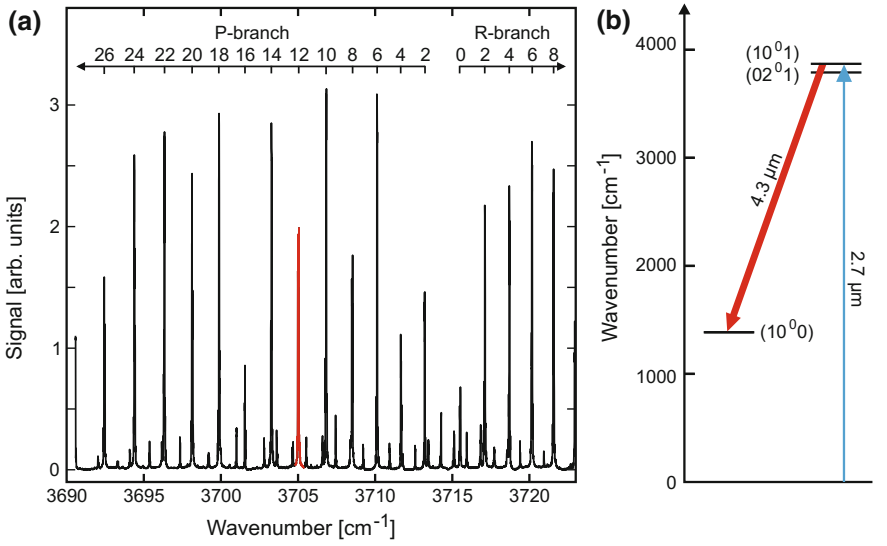

Fig. 6.4 **a** Measured rotational-vibrational excitation spectrum of CO_2 at 27 °C. The P12 is indicated in the figure and was used for excitation with a laser wavelength of 2.7 μm. **b** Energy diagram of the CO_2 molecule and the excitation by the laser sheet and the resulting fluorescence which was detected at 4.3 μm

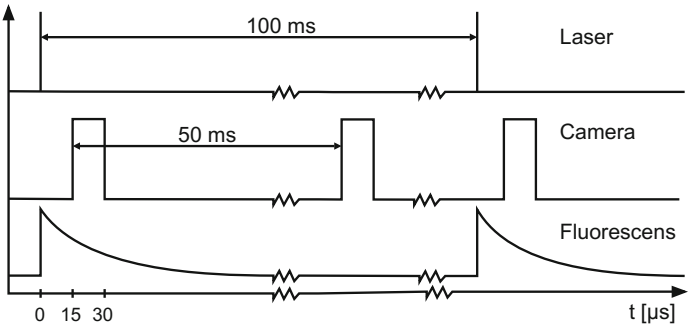

Fig. 6.5 Illustration of the time triggering scheme between the laser and the camera to remove the thermal background

delay relative to the Q-switch of the laser. In Fig. 6.5 it can be seen that the laser sets the start time and the fluorescence appears almost instantly. The camera is then triggered 15 µs after the opening of the laser Q-switch. The exposure time for the camera is optimized to discriminate background and favor fluorescence signal and set to 15 µs. The camera is then triggered once more during the cycle 50 ms after the first exposure, camera gate unchanged. This is to collect the thermal background without any influence of the laser. 100 ms after the first laser shot the next cycle starts, again with the opening of the laser Q-switch.

The fluorescence signal was collected by a CaF_2 lens at 90° to the incident laser sheet through a narrowband, liquid-nitrogen-cooled, interference filter (centered at 4.26 µm) and detected by a 256 × 256 InSb IR camera (Santa Barbara Focal Plane, SBF LP134). Using this set-up, our detection limit of CO_2 is at present 100 ppm or 0.1 mbar at a total pressure of 100 mbar.

6.3.1 One Sample: CO_2 Imaging Above a Pd(100) Single Crystal

The Pd(100) single-crystal surface is one of the most commonly used substrates as a model catalyst to study CO oxidation under semi-realistic conditions. The surface structure during the reaction has been studied with Scanning Tunneling Microscopy (STM) [11], X-ray Photoelectron Spectroscopy (XPS) [21], (High Energy) Surface X-Ray Diffraction ((HE)SXRD) [12, 24], Infrared Reflection Absorption Spectroscopy (IRAS) [15], and extensively by Density Functional Theory (DFT) calculations [25–29]. The experimental surface studies are done with simultaneous mass spectrometry data collection to relate the state of the surface with the activity of the sample, and all of the experiments are performed using reactors similar to the one described above and used in the present experiments. Despite using mass spectrometry, it is in general difficult to visualize the gas-phase distribution in such a reactor, in particular when the model catalyst becomes active.

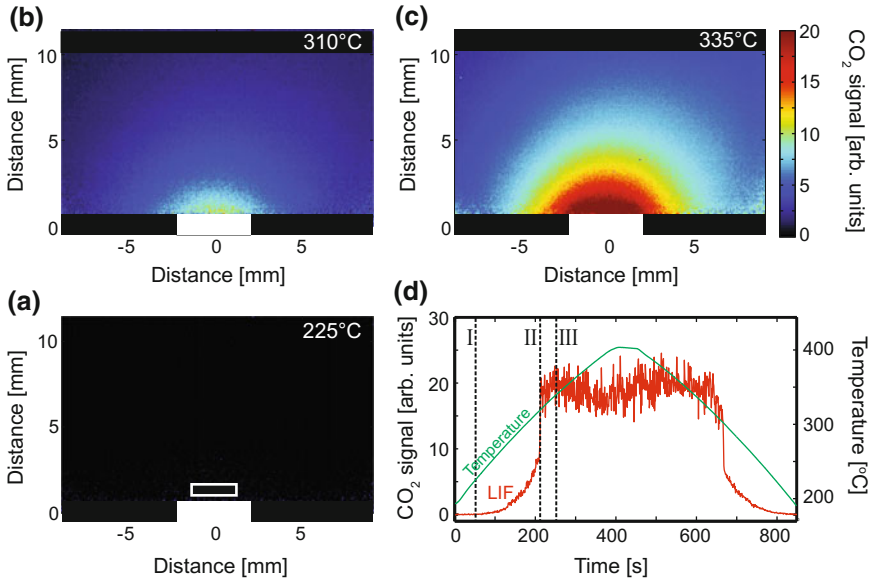

Fig. 6.6 A Pd(100) single crystal (indicated by the filled white rectangle) in a flow of 4 ml/s CO and 4 ml/s O_2 at a temperature of **a** 225 °C, **b** 310 °C, and **c** 335 °C. **d** The temperature (*green*) during the experiment and the LIF signal (*red*) extracted from the area indicated by a small non-filled rectangle

In Fig. 6.6 an experiment using a flow of 4 ml/min CO, 4 ml/min O_2 and 92 ml/min Ar through the reactor above a Pd(100) single-crystal model catalyst is shown. During the experiment, the temperature is first increased and later decreased (Fig. 6.6d) while the CO_2 LIF signal (Fig. 6.6d) from a point 1 mm above the sample is monitored. In Fig. 6.6a–c, 2D PLIF images of the CO_2 fluorescence as seen from the side of the crystal are shown at different temperatures. At a temperature of 225 °C, no signal can be detected as seen in Fig. 6.6a. However, as the temperature is increasing, a slow increase in the activity can be observed in the LIF signal. At a critical temperature, there is a sudden CO_2 increase, and 2D PLIF images at the transition are shown in Fig. 6.6b, c. In Fig. 6.6c a significant amount of CO_2 is observed, directly showing the formation of a CO_2 cloud in the form of a so-called boundary layer. As the temperature is increased further, the CO_2 production is constant at a high value. From these images alone it is evident that the gas-phase composition in the vicinity of the Pd(100) surface is very different from the gas composition introduced by the mass flow controllers, and as a result, the surface composition of the model catalyst is not reflected by the introduced gas composition, but rather by the local gas composition close to the catalyst surface. Furthermore, the CO_2 production becomes constant despite increasing the temperature. The reason for this is that, under these conditions, the oxidation of the CO at the surface is faster than the CO flow to the surface, leading to the build-up of the CO_2 boundary layer. It is said that the catalyst

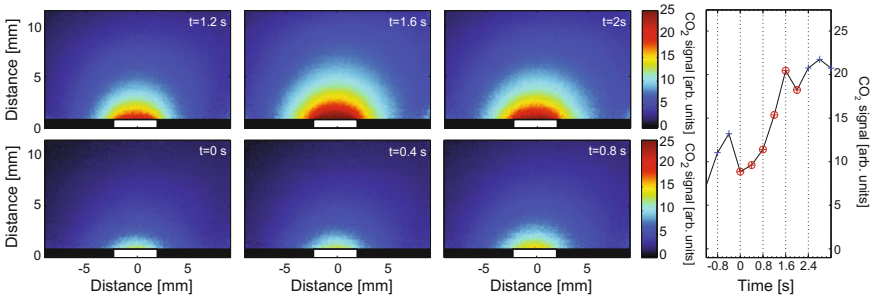

Fig. 6.7 CO_2-tuned PLIF images recorded with a 0.4 s resolution above a Pd(100) single crystal as the reaction ignites. Any region of interest in the images can be plotted as a function of time. The *right panel* shows the LIF intensity just above the sample

is in a Mass Transfer Limited (MTL) regime, which can also be observed by mass spectrometry and other methods [13, 15, 21]. However, the visual 2D information that the PLIF imaging provides generates a new and complementary experimental view and a direct understanding of this phenomenon.

The observation of a sudden change in the CO_2 production clearly suggests a change in the reaction pathway at the surface, suggesting a change of the adsorbed molecules or in the surface structure. The most likely scenario is the desorption of CO and/or a resulting oxidic (chemisorbed/oxide) layer on the surface.

The relatively high time resolution (see Fig. 6.7) of the PLIF imaging enables the extraction of the CO_2 concentration at an arbitrary position in the 2D images and to simultaneously follow the CO_2 change when conditions such as the temperature or the gas composition are changing, as long as the corrections of the LIF intensity as described above are taken into account. Each image in Fig. 6.7 is an average of four consecutive PLIF images with 0.1 s resolution. For instance, with a proper treatment of the background levels in the images, it is possible to extract Arrhenius plots to obtain activation energies for a certain catalyst under investigation.

6.3.2 Two Samples

An attractive property of the PLIF measurements as performed in the present experiments is the 2D character of the imaging. As a result, a spatial resolution of the gas phase of around 0.4 mm can easily be achieved, and therefore it is possible to study inhomogeneous samples or to directly compare the activity of two different samples.

In Fig. 6.8 two different powder catalysts, indicated by the white filled squares, are studied in the same way as the single-crystal Pd sample shown above. The right-hand sample contains 2% (by weight) of Pd in CeO_2 while the left hand sample contains 2% of Pt and 1% of Pd also in CeO_2 as indicated in the bottom panel of Fig. 6.8a. The samples are separated by approximately 8 mm. By taking images with a high time resolution and increasing the temperature continuously of both samples

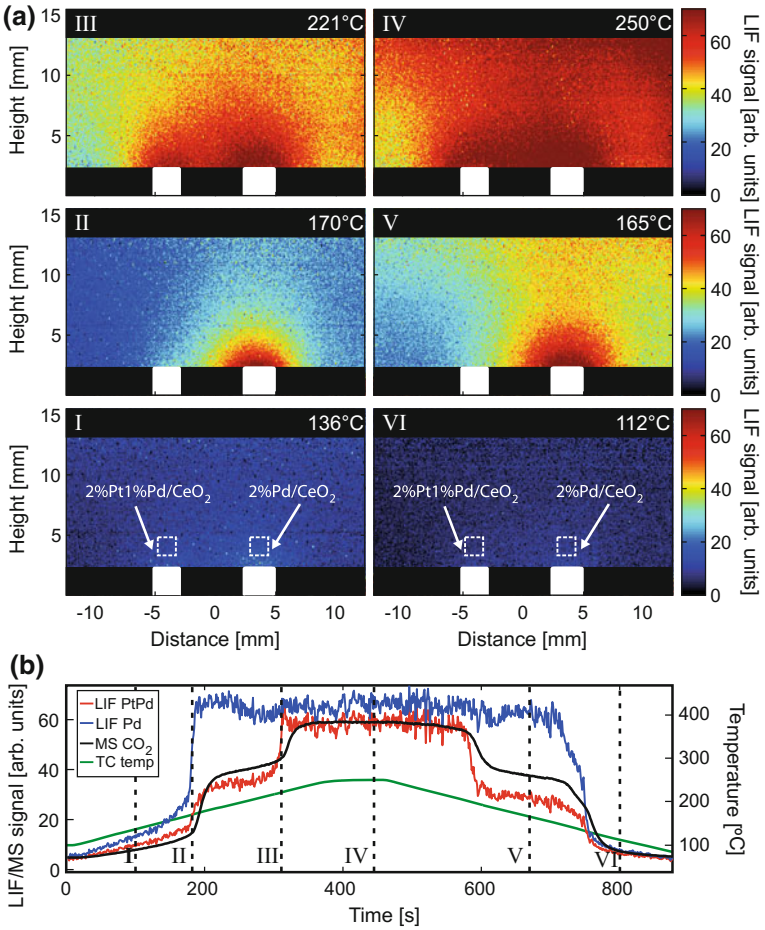

Fig. 6.8 A CO oxidation experiment imaging the CO_2 fluorescence above two powder catalysts (2%Pt1%Pd/CeO_2 and 2%Pd/CeO_2) in the reactor. **a** PLIF images collected at increasing temperatures (*I–III*) and decreasing temperatures (*IV–VI*). It is immediately clear that the 2%Pd/CeO_2 starts to produce CO_2 at a lower temperature than the 2%Pt1%Pd/CeO_2 sample. **b** The LIF signal from the indicated non-filled white squares in Fig. 6.8a *I* and *VI*, as well as the temperature. The mass spectrometer signal has been added for comparison

simultaneously in the same gas flow, we can evaluate the difference in activity of the samples. From the 2D images in Fig. 6.8a, showing snapshots during the experiment, it is directly clear that the 2%Pd/CeO_2 powder sample reaches the MTL, and is thus highly active, at a temperature which is approximately 55 °C lower than for the 2%Pt%Pd/CeO_2 sample. The CO_2 mass spectrometry signal overlaid on the PLIF signals in Fig. 6.8b has a similar, but smeared-out, profile as the PLIF signal from the 2%Pt%Pd/CeO_2 sample. The reasons for the lower activation temperature for the 2%Pd/CeO_2 powder sample could be many, and would require structural characterization of the catalysts, which is beyond the scope of the present chapter, in which we

instead focus on the capabilities of PLIF. Nevertheless, the measurements in Fig. 6.8a show an interesting potential for direct comparison between the catalytic properties of different catalysts for screening purposes.

However, it is also clear from the 2D images, and in particular the point measurements directly above the catalysts as shown in Fig. 6.8b, that there is a spill-over effect from the 2%Pd/CeO_2 powder sample as it becomes active to the 2% Pt%Pd/CeO_2 sample. In experiments performed for the same samples but only one sample at a time, while no difference for the 2%Pd/CeO_2 sample was observed, the 2%Pt%Pd/CeO_2 became highly active and deactivated at temperatures different from when being in the presence of the 2%Pd/CeO_2 sample. Thus, we conclude that the gas diffusion generated by the sample with the lowest activation temperature affects the sample which becomes active at higher temperature.

6.3.3 Three Tubes

For practical purposes and if high accuracy is needed in determining differences in catalytic activity, it is necessary to separate the catalysts to avoid any spill-over effects. Such an experiment was performed by probing the exhaust from three separated glass-tubes inside the reactor chamber. In the glass-tubes, different catalysts were placed and the gas was directed to flow through the three tubes. The tubes ended inside the middle of the vacuum chamber where the laser sheet was placed as close as possible (<1 mm) to the exits of the tubes. The gas flow was kept the same through all three tubes, and the temperature was increased equivalently by a heating tape around the tubes, and measured by a thermocouple situated between the tubes. This solution enables an independent measurement of the CO_2 production from each catalyst under the same conditions.

The results are shown in Fig. 6.9 for powder catalysts consisting of 2%Pd/CeO_2, 2%Pt/CeO_2 and 2%Pt/Al_2O_3 dispersed on monoliths with the same diameter as the glass tubes. At low temperature, none of the catalysts produces CO_2 as can be seen in Fig. 6.9a, panel I. However, as the temperature is increased, the catalysts become active in CO_2 production, starting with the Pd/CeO_2 at 180 °C, the Pt/CeO_2 at 280 °C, and the Pt/Al_2O_3 catalyst at 350 °C, in Fig. 6.8a panels II, III, and IV, respectively. The mass spectrometry also detects changes in the CO_2 production but is unable to detect which of the samples becomes active at a certain temperature. In this case it is possible to extract the activation energies from the LIF signal by producing an Arrhenius plot from the development of the CO_2 production at the outlet of each tube.

The above experiment using three exhaust tubes separating product gas from each sample is an example on how PLIF may be used to discriminate between different catalysts. The example enables a direct view of the amount of the products at a given temperature. It is, however, clear that the experimental set-up can be modified and simplified to a large extent, and may have potential for practical use.

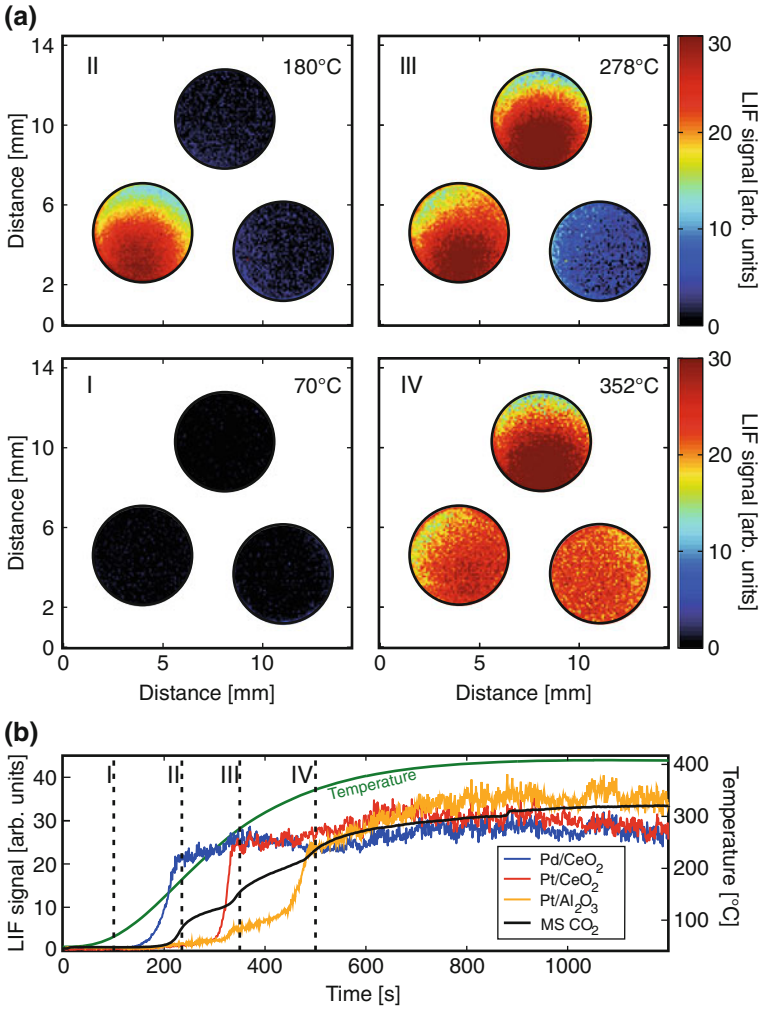

Fig. 6.9 An experiment using three exhaust tubes containing active CO oxidation powder catalysts (Pd/CeO_2, Pt/CeO_2 and Pt/Al_2O_3) exiting in the vacuum PLIF reactor imaging the CO_2 fluorescence just above the tubes simultaneously. **a** PLIF images as the temperature of the tubes is increasing from 70 to 352 °C. **b** Extracted LIF intensity at the outlet of each tube as a function of temperature. The CO_2 mass spectrometry signal is added as a reference

6.4 CO Imaging

Electronic CO resonances are located in the VUV regime and LIF is obtained via two-photon excitation in the $B^1\sum^+ \longleftarrow X^1\sum(0,0)$ Hopfield-Birge band using 230 nm (see Fig. 6.10a [2]), followed by population of the A-state via collisions or radiative transitions with fluorescence emission bands in the wavelength range 450–

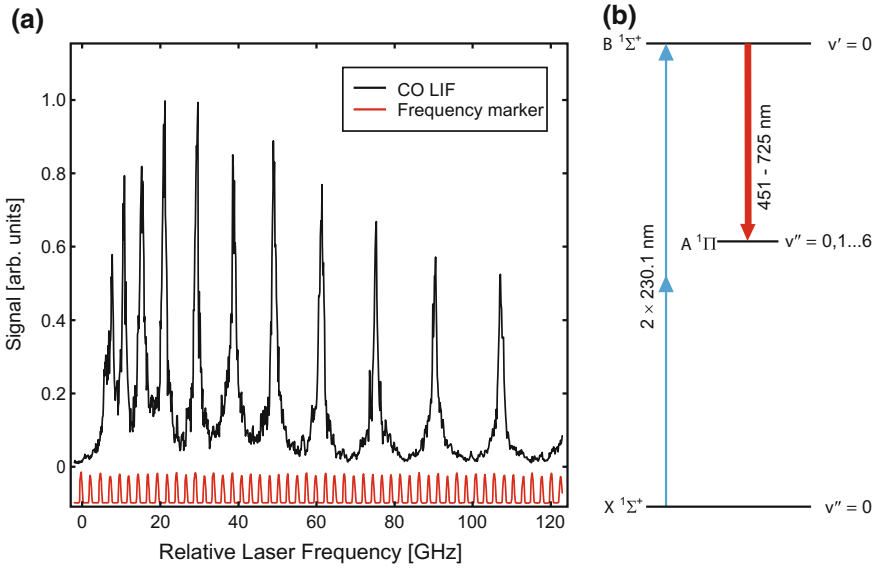

Fig. 6.10 **a** Excitation scan of CO gas at 50 mbar [2] (115 nm). **b** Schematic drawing of the two-photon excitation of the CO molecule and the subsequent decay by fluorescence at different wavelength [2]

660 nm, see Fig. 6.10b. Using a picosecond laser system consisting of a mode-locked Nd:YAG laser (PL2143C, Ekspla) with external amplifier (APL70–1100, Ekspla), these band states could be excited. We use the Nd:YAG third harmonic at 355 nm to pump an Optical Parametric Generator (PG 401-P80-SH, Ekspla), tuned to 230 nm. The pulse duration was 80 ps, the laser pulse repetition rate 10 Hz, and the line width at 230 nm was specified to 5 cm^{-1}. For CO PLIF imaging the 230 nm laser beam was directed through the reactor and shaped into a 7 mm high vertical sheet using two cylindrical lenses of focal lengths f = +500 mm and f = +300 mm. Images were acquired using an f = 50 mm objective (Nikkor f/1.2) and a 36 mm extension tube mounted on an ICCD camera (PIMAX III, Princeton Instruments). Images were acquired at 10 Hz repetition rate every 100 ms with the intensifier gate set to 30 ns. A longpass filter (GG395, Schott) was used to suppress scattering and fluorescence from surfaces in the reactor. The CO pressures were calibrated by using gas mixtures of well-defined CO partial pressures at a reactor temperature of 150 °C.

6.4.1 CO Imaging Above a Pd(110) Single Crystal

Figures 6.11a, b, and c show CO PLIF images of the gas phase above a Pd(110) single crystal in partial pressures of 26.5 mbar CO, 26.5 mbar O_2, and 53 mbar Ar, yielding

a total pressure of 106 mbar in the reactor, at temperatures of 300 °C, 365 °C, and 375 °C, respectively. At 300 °C a significant CO fluorescence can be detected while a decreasing CO signal can be observed at 370 °C, indicating an onset of the CO_2 oxidation reaction. At 370 °C the CO signal is significantly reduced in the vicinity of the Pd(110) sample, suggesting that the surface is in a highly active state. Fig. 6.11d shows the intensity of the LIF signal in the area just above the sample indicated in Fig. 6.11a, b and c. Here a prominent decrease of the CO signal is confirmed above 370 °C reaching a low-level plateau which is unaffected by further temperature increase, demonstrating a MTL reaction rate. A similar, but less pronounced behavior can be seen in the CO mass spectrometry signal.

It is gratifying to see that the CO signal is behaving opposite to that of the CO_2 signal observed in the case of CO_2 imaging above the Pd(100) sample, which was shown in Fig. 6.6. However, it is also clear that during the highly active state the CO partial pressure is significantly different close to the Pd(110) surface as compared to at the outlet, where the MS is located. While the CO partial pressure decreases by 80% 0.3 mm above the Pd(110) surface as the sample becomes active, the decrease is only 20–30% 9 mm away from the sample which is similar to the condition where the MS is located. These observations emphasize the fact that studying model catalysts in a high-speed reaction such as CO oxidation in a vacuum chamber using semi-realistic conditions demands gas-phase measurements in direct vicinity of the catalyst.

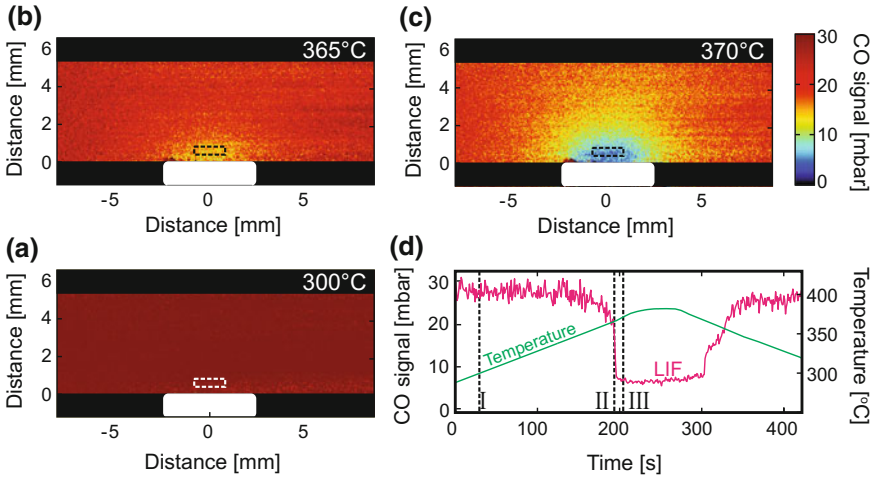

Fig. 6.11 CO LIF images (averages over ten single-shot frames) from a Pd(110) crystal in a gas composition of 26.5 mbar CO, 26.5 mbar O_2, and 53 mbar Ar at **a** 300 °C, **b** 365 °C, **c** 370 °C. **d** LIF intensity plot (*red*) from the indicated non-filled square in the LIF images and the temperature (*green*)

6.5 NH_3 Imaging

The potential to use PLIF to image the gas phase surrounding an active catalyst is significant. At present, only one gas species can be probed for each experiment. However, the experience from other research areas, such as combustion physics, in handling all aspects of laser techniques makes it possible to probe a large number of molecules important for catalysis. As an example, we present how NH_3 can be imaged by PLIF as it takes part in a catalytic reaction.

In the case of the NH_3 presented here, two-photon LIF was used as has been described elsewhere [37]. In Fig. 6.12a an excitation scan of the NH_3 molecules is shown. The simultaneous absorption of two photons allows for excitation wavelengths in the visible regime facilitating the detection capabilities. To this end, a combined Nd:YAG (Quanta-Ray PRO 250-10, Spectra Physics) and dye laser (Cobra Stretch-G-2400, Sirah) system operating at 10 Hz repetition rate and with 8 ns pulse duration was used for two-photon excitation of NH_3. The fluorescence emission spectrum is shown in Fig. 6.12b, showing best detection capabilities at wavelengths around 565 nm which for the present LIF measurements was detected with an intensified CCD camera (PI-MAX3, Princeton Instruments). A schematic of the two-photon excitation and the fluorescence emission is shown in Fig. 6.12c.

6.5.1 NH_3 Oxidation Above a Ag/Al_2O_3 Powder Catalyst

The investigation of the oxidation of NH_3 is part of a project to investigate the NO reduction reaction in an oxidizing environment using Ag-based catalysts [38] and NH_3 or hydrocarbons as a reducing agent. Since the NO reduction by NH_3 or a hydrocarbon, and the oxidation of NH_3 or the hydrocarbon by oxygen is competing, it is also of interest to study the NH_3 oxidation. In the present investigation, we used a Ag/Al_2O_3 powder catalyst to study the abundance of NH_3 in different envi-

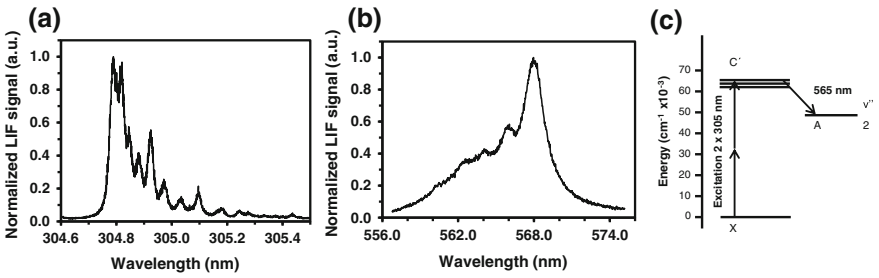

Fig. 6.12 **a** Excitation scan of the NH_3 molecules. **b** Fluorescence emission spectrum from NH_3 gas [37]. **c** Schematics of the two-photon excitation and fluorescence detection energies used in the present measurements

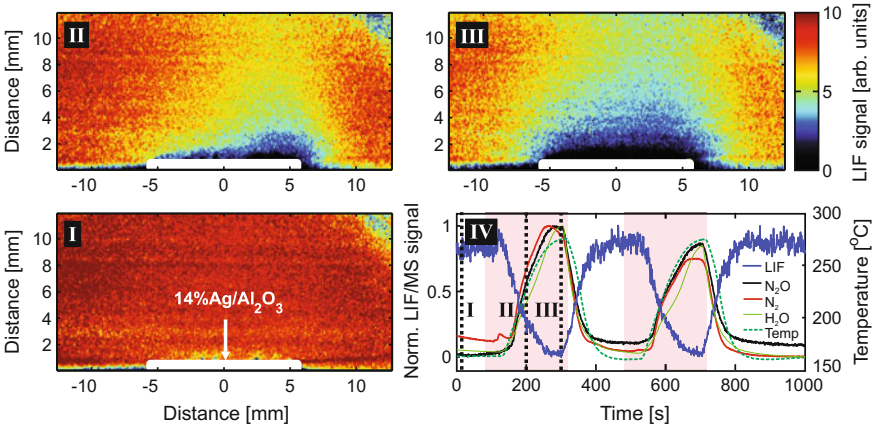

Fig. 6.13 NH_3 imaging (*panels I–III*) above a Ag/Al_2O_3 powder catalyst at a constant temperature of 160 °C and relevant mass spectrometry signals (*panel IV*). At 0 s a homogenous NH_3 distribution is observed. As soon as the H_2 is introduced (indicated by *red*), the NH_3 signal is depleted, reaching a minimum after 300 s, when the H_2 is evacuated

ronments. In particular, the experiments illustrate the promotional effect of H_2 on the oxidation of NH_3. The oxidation of NH_3 may follow several reaction pathways, for example

$$\mathbf{2NH_3 + 3/2O_2 \Rightarrow N_2 + 3H_2O}$$
$$\mathbf{2NH_3 + 5/2O_2 \Rightarrow 2NO + 3H_2O}$$
$$\mathbf{2NH_3 + 7/2O_2 \Rightarrow 2NO_2 + 3H_2O}$$

In Fig. 6.13 we show an experiment using a Ag/Al_2O_3 powder catalyst inside the reactor at a temperature of approximately 160 °C in a mixture of 3.6% NH_3, 90% O_2 with pulses of 6% Ar or H_2. The PLIF images are shown in panels I-III, and after 10 s of constant pressures the NH_3 distribution appears homogenous above the catalyst. However, as soon as H_2 is introduced into the reactor, the NH_3 LIF signal just above the catalyst starts to decrease in intensity and after 200 s it is clearly visible in panel II as a depletion of the signal. This observation indicates oxidation of the NH_3. The depletion of the NH_3 signal reaches its minimum after 300 s, when the H_2 is evacuated from the reactor, and the NH_3 signal increases to its original value. The LIF signal from a region of interest just above the catalyst is also shown in panel IV, as well as the mass spectrometry signals of N_2, H_2O, and N_2O, and the temperature.

It is clear from the PLIF NH_3 images that the NH_3 distribution is not even across the catalyst surface when the H_2-assisted oxidation initiates. The reasons for this could be either an uneven distribution of the active catalyst material, or it could be due to slight inhomogeneities in the temperature distribution of the sample.

6.6 Summary

PLIF in combination with the current fast development of laser and imaging technology has provided a new 2D-view on catalysis. Our initial driving force has been the urge to provide a 2D visualization of the CO_2 distribution around a single-crystal model catalyst during a CO oxidation experiment in semi-realistic conditions, to understand previous surface-science-based *in situ* results.

The present chapter demonstrates that it is currently possible, without too much effort, to measure the CO_2 signal during a CO oxidation experiment, providing that expertise in both laser diagnostics and catalysis-related research is combined. By choosing the right laser and detector combination, the 2D CO_2 distribution can be followed on a timescale faster than 0.4 s. This enables one to directly follow the ignition of the CO_2 production from single crystals or technical powder catalysts and the direct 2D visualization of the CO_2 boundary layer at MTL conditions, which demonstrates the substantial differences in gas composition close to the catalyst as compared to far away from the catalyst. The 2D-aspect of CO_2 PLIF imaging also enables a direct view of the CO_2 ignition of two samples in the same reactor, differentiating between their ignition temperatures. Furthermore, the chapter also provides indications on how spill-over effects can be avoided by introduction of exhaust tubes into the reactor.

Similarly, by the use of the correct laser and detection system, the 2D CO distribution in the same reaction can also be visualized and measured. Here, the intensity variation is inverted as compared to the CO_2 measurements, and directly explains observations made by previous high-pressure XPS measurements.

Finally, this chapter also describes how to perform PLIF measurements from NH_3 as it is oxidized in a catalytic oxidation reaction above a powder catalyst.

It is clear that PLIF applied to catalysis is not limited to the molecules probed in the present chapter. The extensive experience from the combustion physics/chemistry community will enable PLIF measurements of most small hydrocarbons as well as from a large range of other molecules as reactants or products in the vicinity of a catalyst for a particular reaction at work. Therefore, the potential benefits of applying PLIF to catalysis, for a better understanding of certain catalytic reactions, to identify intermediates only present in the gas phase in the vicinity of the catalyst, for potential commercial applications, and for combining with other experimental *in situ* techniques to simultaneously probe the presence of surface species is enormous.

Acknowledgements This work was financially supported by the foundation for strategic research (SSF), the Swedish Research Council, the Crafoord Foundation, the Knut and Alice Wallenberg Foundation, the Anna and Edwin Berger Foundation and NordForsk.

References

1. S. Svanberg, Phys. Scripta **T19b**, 469 (1987)
2. M. Aldén, S. Wallin, W. Wendt, Appl. Phys. B-Photo **33**, 205 (1984)
3. A.C. Eckbreth, *Laser Diagnostics for Combustion Temperature and Species, Abacus Press* (Kent; Cambridge, Mass, Tunbridge Wells, 1988)
4. E. Fridell, U. Westblom, M. Aldén, A. Rosén, J. Catal. **128**, 92 (1991)
5. E. Fridell, A.P. Elg, A. Rosén, B. Kasemo, J. Chem. Phys. **102**, 5827 (1995)
6. E. Fridell, A. Rosén, B. Kasemo, Langmuir **10**, 699 (1994)
7. F. Gudmundson, J.L. Persson, M. Forsth, F. Behrendt, B. Kasemo, A. Rosén, J. Catal. **179**, 420 (1998)
8. W. Kang, O. Fujita, K. Ito, J. Energ. Resour-Asme. **118**, 82 (1996)
9. F. Gudmundson, E. Fridell, A. Rosén, B. Kasemo, J. Phys. Chem-Us **97**, 12828 (1993)
10. H. Su, E.S. Yeung, J. Am. Chem. Soc. **122**, 7422 (2000)
11. B.L.M. Hendriksen, S.C. Bobaru, J.W.M. Frenken, Surf. Sci. **552**, 229 (2004)
12. R. van Rijn, O. Balmes, A. Resta, D. Wermeille, R. Westerstrm, J. Gustafson, R. Felici, E. Lundgren, J.W.M. Frenken, Phys. Chem. Chem. Phys. **13**, 13167 (2011)
13. J. Gustafson, R. Westerström, A. Mikkelsen, X. Torrelles, O. Balmes, N. Bovet, J.N. Andersen, C.J. Baddeley, E. Lundgren, Phys. Rev. B **78**, 045423 (2008)
14. R. Westerström, J.G. Wang, M. Ackermann, J. Gustafson, A. Resta, A. Mikkelsen, J.N. Andersen, E. Lundgren, O. Balmes, X. Torrelles, J.W.M. Frenken, B. Hammer, J. Phys.: Condens. Matter **20**, 184019 (2008)
15. F. Gao, S.M. McClure, Y. Cai, K.K. Gath, Y. Wang, M.S. Chen, Q.L. Guo, D.W. Goodman, Surf. Sci. **603**, 65 (2009)
16. F. Gao, Y. Wang, Y. Cai, D.W. Goodman, J. Phys. Chem. C **113**, 174 (2009)
17. J. Gustafson, R. Westerström, A. Resta, A. Mikkelsen, J.N. Andersen, O. Balmes, X. Torrelles, M. Schmid, P. Varga, B. Hammer, G. Kresse, C.J. Baddeley, E. Lundgren, Catal. Today **145**, 227 (2009)
18. J. Gustafson, R. Westerström, O. Balmes, A. Resta, R. van Rijn, X. Torrelles, C.T. Herbschleb, J.W.M. Frenken, E. Lundgren, J. Phys. Chem. C **114**, 4580 (2010)
19. J. Gustafson, R. Westerström, O. Balmes, A. Resta, X. van Rijn, R. Torrelles, C.T. Herbschleb, J.W.M. Frenken, E. Lundgren, J. Phys. Chem. C **114**, 22372 (2010)
20. R. Toyoshima, M. Yoshida, Y. Monya, Y. Kousa, K. Suzuki, H. Abe, B.S. Mun, K. Mase, K. Amemiya, H.J. Kondoh, Phys. Chem. C **116**, 18691 (2012)
21. S. Blomberg, M.J. Hoffmann, J. Gustafson, N.M. Martin, V.R. Fernandes, A. Borg, Z. Liu, R. Chang, S. Matera, K. Reuter, E. Lundgren, Phys. Rev. Lett. **110**, 117601 (2013)
22. R. Toyoshima, M. Yoshida, Y. Monya, K. Suzuki, K. Amemiya, K. Mase, B.S. Mun, H. Kondoh, J. Phys. Chem. C **117**, 20617 (2013)
23. J. Gustafson, S. Blomberg, N.M. Martin, V. Fernandes, A. Borg, Z. Liu, R. Chang, E. Lundgren, J. Phys.: Condens. Matter **26**, 055003 (2014)
24. J. Gustafson, M. Shipilin, C. Zhang, A. Stierle, U. Hejral, U. Ruett, O. Gutowski, P.A. Carlsson, M. Skoglundh, E. Lundgren, Science **343**, 758 (2014)
25. J. Rogal, K. Reuter, M. Scheffler, Phys. Rev. Lett. **98**, 046101 (2007)
26. J. Rogal, K. Reuter, M. Scheffler, Phys. Rev. B **77**, 155410 (2008)
27. S. Matera, K. Reuter, Catal. Lett. **133**, 156 (2009)
28. S. Matera, K. Reuter, Phys. Rev. B **82**, 035410 (2010)
29. Z. Duan, G. Henkelman, ACS Catal. **4**, 3435 (2014)
30. J. Zetterberg, S. Blomberg, J. Gustafson, Z.W. Sun, Z.S. Li, E. Lundgren, M. Aldén, Rev. Sci. Instrum. **83**, 053104 (2012)
31. B.J. Kirby, R.K. Hanson, Appl. Optics. **41**, 1190 (2002)
32. B.J. Kirby, R.K. Hanson, Appl. Optics. **40**, 6136 (2001)
33. Z.S. Li, M. Rupinski, J. Zetterberg, Z.T. Alwahabi, M. Aldén, Chem. Phys. Lett. **407**, 243 (2005)

34. B.J. Kirby, R.K. Hanson, Proc. Combust. Inst. **28**, 253 (2000)
35. J.T. Houghton, P. Phys, Soc. London **91**, 439 (1967)
36. W.A. Rosser, A.D. Wood, E.T. Gerry, J. Chem. Phys. **50**, 4996 (1969)
37. C. Brackmann, O. Hole, B. Zhou, Z.S. Li, M. Aldén. Appl. Phys. B **115**, 25 (2014)
38. F. Thibault-Starzyk, E. Seguin, S. Thomas, M. Daturi, H. Arnolds, D.A. King, Science **324**, 1048 (2009)